The scaling properties of two-dimensional compressible magnetohydrodynamic turbulence

J. A. Merrifield, T. D. Arber, S. C. Chapman, and R. O. Dendy

Citation: Physics of Plasmas (1994-present) **13**, 012305 (2006); doi: 10.1063/1.2149762
View online: http://dx.doi.org/10.1063/1.2149762
View Table of Contents: http://scitation.aip.org/content/aip/journal/pop/13/1?ver=pdfcov
Published by the AIP Publishing

The scaling properties of two-dimensional compressible magnetohydrodynamic turbulence

J. A. Merrifield, T. D. Arber, and S. C. Chapman
Department of Physics, University of Warwick, Coventry CV4 7AL, United Kingdom

R. O. Dendy[a)]
UKAEA Culham Division, Culham Science Centre, Abingdon, Oxfordshire OX14 3DB, United Kingdom

(Received 26 October 2005; accepted 16 November 2005; published online 12 January 2006)

Understanding the phenomenology captured in direct numerical simulation (DNS) of magnetohydrodynamic (MHD) turbulence rests upon models and assumptions concerning the scaling of field variables and dissipation. Here compressible MHD turbulence is simulated in two spatial dimensions by solving the isothermal equations of resistive MHD on a periodic square grid. In these simulations it is found that the energy spectrum decreases more slowly with k, and the viscous cutoff length is larger, than would be expected from the 1941 phenomenology of Kolmogorov (K41). Both these effects suggest that the cascade time is modified by the presence of Alfvén waves as in the phenomenology of Iroshnikov and Kraichnan (IK). Motivated by this, these scaling exponents are compared with those of the IK-based model of Politano and Pouquet [Phys. Rev. E **52**, 636 (1995)], which is an extension of the model of She and Leveque [Phys. Rev. Lett. **72**, 336 (1994)]. However, the scaling exponents from these simulations are not consistent with the model of Politano and Pouquet, so that neither IK nor K41 models would appear to describe the simulations. The spatial intermittency of turbulent activity in such simulations is central to the observed phenomenology and relates to the geometry of structures that dissipate most intensely via the scaling of the local rate of dissipation. The framework of She and Leveque implies a scaling relation that links the scaling of the local rate of dissipation to the scaling exponents of the pure Elsässer field variables ($\mathbf{z}^{\pm}=\mathbf{v}\pm\mathbf{B}/\sqrt{\mu_o\rho}$). This scaling relation is conditioned by the distinct phenomenology of K41 and IK. These distinct scaling relations are directly tested using these simulations and it is found that neither holds. This deviation suggests that additional measures of the character of the dissipation may be required to fully capture the turbulent scaling, for example, pointing towards a refinement of the phenomenological models. It may also explain why previous attempts to predict the scaling exponents of the pure Elsässer fields in two-dimensional magnetohydrodynamic turbulence by extending the theory of She and Leveque have proved unsuccessful. © *2006 American Institute of Physics*. [DOI: 10.1063/1.2149762]

I. INTRODUCTION

Magnetohydrodynamic (MHD) flows display turbulent behavior when the conditions $R_v=l_0v_{\mathrm{std}}/\nu\gg 1$ and $R_B=l_0v_{\mathrm{std}}/\eta\gg 1$ are satisfied. Here l_0 is the integral length scale of the flow (e.g., a macroscopic driving scale), v_{std} is the velocity field standard deviation, ν is the kinematic viscosity, η is the magnetic diffusivity, and R_v and R_B are the kinetic and magnetic Reynolds numbers, respectively. It has long been suggested that the turbulent state can be understood in terms of the spatial scaling of its statistical properties. Perhaps the best known characterization of spatial scaling in turbulent media is the energy spectrum, which is essentially a second-order statistical measure. The Kolmogorov phenomenology,[1] (K41) assumes that the nonlinear interaction dominating the cascade process is eddy scrambling, while that of Iroshnikov and Kraichnan[2,3] (IK) assumes that the dominant process is Alfvén wave collisions.[4] Kolmogorov predicted that the energy spectrum should scale as $\sim k^{-5/3}$ while Iroshnikov-Kraichnan predicted that it should scale as $\sim k^{-3/2}$. A Kolmogorov-type energy spectrum, with wave vectors taken perpendicular to the local magnetic field, can also be derived from Alfvén wave collisions providing that the assumption of *critical balance* is valid after the work of Goldreich and Sridhar.[5] However, numerical evidence suggests that this condition is not satisfied in two-dimensional (2D) MHD.[6]

In the present work we implement the equations of isothermal compressible MHD directly in two spatial dimensions and then evaluate the applicability of the K41 and IK phenomenologies by determining the relevant scaling relations. We introduce other scaling relations in Sec. II of this paper, which characterize the spatial intermittency of turbulent activity in terms of statistics of higher than second order. We compare our work with other two-dimensional MHD turbulence simulations where high-order statistics are calculated; chiefly Refs. 7–9. Reference 7 deals with freely decaying incompressible turbulence, while Refs. 8,9 deal with incompressible turbulence driven into a quasistationary state. Of interest is the fact that the scaling exponents reported from the driven and decaying studies do not entirely agree

[a)]Also at Department of Physics, University of Warwick, Coventry CV4 7AL, UK.

with each other, even though they are both run at reasonably high Reynolds numbers. One may speculate either that 2D turbulence driven into a quasistationary state fundamentally differs from decaying turbulence or that some nonuniversality is present in 2D MHD turbulence. However, both 2D studies yield scaling exponents that appear to imply greater intermittency than those found in three-dimensional (3D) decaying MHD turbulence.[10] We pay particular attention to the combined scaling properties of the Elsässer field variables $\mathbf{z}^{\pm} \equiv \mathbf{v} \pm \mathbf{B}(\mu_0 \rho)^{-1/2}$ and the local rate of dissipation which, as we shall see, bear particular relevance to currently favored models for intermittency. Crucially, these models rely on an assumed link between the scaling properties of the Elsässer field variables and the local rate of dissipation. Focusing on these combined scaling laws allows us to quantify how far this assumption is valid.

We find that the K41 phenomenology does not describe our simulation of 2D MHD turbulence. This finding is consistent with previous studies.[6–8,11] In particular, we find that the energy spectrum decreases more slowly with k, and the viscous cutoff length is larger, than would be expected from K41. Both these effects can be attributed to the modification of the energy cascade by the presence of Alfvén waves—a process that is central to the IK phenomenology. However, the scaling properties that we recover are also not completely compatible with the IK phenomenology. In particular, we find that the scaling of the pure Elsässer field variables ($\mathbf{z}^+$ or $\mathbf{z}^-$) does not agree with the IK-based intermittency model of Ref. 12. This was also found in Refs. 7,8. We note that no intermittency model that describes the scaling behavior of the pure Elsässer fields, based on the 1994 paper of She and Leveque,[13] has been identified in 2D MHD, although this has achieved much recent success in 3D studies.[10,14–17] Interestingly, Gomez *et al.*[9] reported that the mixed object called the *flux function*, which is a nonlinear combination of the mixed Elsässer field variables $\mathbf{z}^+$ and $\mathbf{z}^-$, displays scaling properties which agree with the original hypothesis of She and Leveque[13]—a model that relies on the K41 phenomenology and most intensely dissipating structures that are filament like. Here, however, we find that analysis of the combined scaling properties of the pure Elsässer field variables and the local rate of dissipation implies that neither the IK- nor K41-based assumptions are valid. This may explain the continuing absence of a robust intermittency model for the pure Elsässer fields.

II. STATISTICAL MEASURES

We normalize magnetic field and density to the characteristic values ρ_0 and B_0 which gives a natural normalization of the velocity to the Alfvén speed $B_0/\sqrt{\mu_0 \rho_0} = v_{A0}$. Time is thus normalized to L_0/v_{A0}. Length is normalized such that the simulation domain size L_0 takes the numerical value of 2π, so that in our periodic system we have a grid spacing of normalized length scales $2\pi/N$, where N is the number of grid points. We thus represent normalized k modes as $k_i = 2\pi m/L_0 = [1, N/2]$ where m is an integer, i.e., k_x and k_y take integer values representing harmonics along their respective directions.

In the construction of energy spectra, we write $k' = \sqrt{k_x^2 + k_y^2}$. The energy spectra considered in the present work are then given by

$$E_v(k) = \frac{1}{2} \sum_{k-0.5 \leqslant k' < k+0.5} |\phi_v(k')|^2, \tag{1}$$

$$E_B(k) = \frac{1}{2} \sum_{k-0.5 \leqslant k' < k+0.5} |\phi_B(k')|^2, \tag{2}$$

$$E(k) = E_B(k) + \bar{\rho} E_v(k), \tag{3}$$

with k taking integer values. Here ϕ_v and ϕ_B are Fourier modes of the $\mathbf{v}$ and $\mathbf{B}$ fields, respectively, with $|\phi_v(k')|$ and $|\phi_B(k')|$ being their amplitudes, and $\bar{\rho}$ is the space averaged mass density. Note that E_v does not relate directly to the kinetic energy $\frac{1}{2}\rho v^2$ but to $\frac{1}{2}\mathbf{v} \cdot \mathbf{v}$, as is conventional in the theory of compressible turbulence.[18] These spectra satisfy the relation

$$\pi^2 \sum_{k=0}^{k=N/2} E(k) = \frac{1}{2} \int_{\mathbf{x}} \{\bar{\rho} v(\mathbf{x})^2 + B(\mathbf{x})^2\} d\mathbf{x}. \tag{4}$$

In recent years attempts have been made to understand turbulence by characterizing the probability density function (PDF) of a fluctuating quantity. For incompressible hydrodynamics the natural choice is the velocity increment $\delta_l v = \mathbf{v}(\mathbf{x}+\mathbf{l}, t) \cdot \mathbf{l}/l - \mathbf{v}(\mathbf{x}, t) \cdot \mathbf{l}/l$, i.e., the instantaneous difference in the velocity field projected along a differencing vector $\mathbf{l}$.[19] Assuming isotropy, the behavior of the hierarchy of PDFs revealed by varying l is described by the scaling properties of structure functions

$$S_v^p(l) = \langle |\delta_l v|^p \rangle, \tag{5}$$

(see, e.g., Ref. 19 and references therein). The angular brackets indicate an ensemble average taken over multiple realizations of the same flow. The averages we calculate here are double averages taken over time t and space $\mathbf{x}$, which are valid for flows which are statistically homogeneous and time stationary. The Elsässer field variables $\mathbf{z}^{\pm} \equiv \mathbf{v} \pm \mathbf{B}(\mu_0 \rho)^{-1/2}$ (in physical units) (Ref. 20) are also of interest for MHD turbulence and we also consider the structure functions of the Elsässer field increments,

$$S_{\pm}^p(l) = \langle |\delta_l z^{\pm}|^p \rangle. \tag{6}$$

Structure functions are sensitive to spatial correlation via dependence on the differencing vector $\mathbf{l}$ and are weighted to events of greater intensity as the order p increases. Statistical self-similarity can be expected in the inertial range $l_0 \gg l \gg l_d$, where l_d is the dissipation scale below which the fluid becomes dissipation dominated. This self-similarity is indicated by scaling laws of the type $S^p(l) \sim l^{\zeta_p}$. The scaling exponents ζ_p are expected to converge to statistically stable values as the Reynolds number approaches infinity—the approximate satisfaction of this asymptotic limit, within experimental error, is termed fully developed turbulence. Frisch[19] describes the statistical properties of very high Reynolds number flows as relating directly to the symmetries present in the equations of motion; this implies universality. The

introduction of an imposed anisotropy, such as an external magnetic field or a large scale shear, could modify the symmetries of the underlying equations of motion that are then reflected in the statistical properties of the flow. Studies of this type are thus ideally performed under isotropic conditions—in real turbulent media this would imply investigating the statistical properties far from any boundaries since these represent an imposed anisotropy. Numerical constraints inhibit the realization of an extensive inertial range in direct simulations, so that $S^p(l) \sim l^{\zeta_p}$. Instead the phenomenon of extended self-similarity[21] (ESS),

$$S^p(l) \sim (S^q(l))^{\zeta_p/\zeta_q} \tag{7}$$

is often considered. While this is found experimentally to extend scaling into the dissipation range down to $\simeq 5l_d$,[22,23] only the ratios of scaling exponents ζ_p/ζ_q can be directly measured by means of Eq. (7).

A further statistical measure is the local rate of dissipation $\epsilon(l,\mathbf{x})$ within a ball of radius l centered on $\mathbf{x}$:

$$\epsilon(l,\mathbf{x},t) = \frac{1}{V}\int_{|\mathbf{x}'-\mathbf{x}|\leq l} \{\epsilon_v(\mathbf{x}+\mathbf{x}',t) + \epsilon_B(\mathbf{x}+\mathbf{x}',t)\} d^E x' . \tag{8}$$

Here V is the volume integrated over, E is the number of Euclidean spatial dimensions, and ϵ_v and ϵ_B are the viscous and Ohmic local rates of dissipation. This quantity is related to $S^p(l)$ insofar as it partly depends upon, and gives information about, the intermittent distribution of eddy activity. Statistical self-similarity in this measure is expressed as $\langle \epsilon(l,\mathbf{x},t)^p \rangle \sim l^{\tau_p}$. Recent experiments and observations concerning hydrodynamic and MHD flows have focused on the one-dimensional (1D) proxy $\chi(l,\mathbf{x},t)$ for $\epsilon(l,\mathbf{x},t)$,

$$\chi_{\pm}(l,\mathbf{x},t) = \frac{1}{l}\int_0^l (\partial_i z_i^{\pm}(x+l',t)^2/\rho) dl' , \tag{9}$$

since many experimental and observational studies return data sets that are only extended along one direction, e.g., Refs 16,22,23. In light of this, computational investigations have also focused on this proxy,[17,24] which we use in the present study.

Scaling arguments from generalized dimensional analyses predict the scaling exponents ζ_p. The K41 (Ref. 1) phenomenology predicts $\zeta_p = p/3$, while IK (Refs. 2,3) predicts $\zeta_p = p/4$.[4] However, these arguments do not account for the spatially intermittent distribution of eddy activity which is found to exist in both hydrodynamic and MHD turbulences, so an intermittency correction is required.

The solar wind represents one of the few high Reynolds number plasmas in which *in situ* measurements are possible.[20] Energy spectra taken from the solar wind routinely return power spectra with indices close to those predicted by the K41 and IK phenomenologies.[25] With this in mind, the solar wind can be interpreted as a turbulent magnetofluid and thus a convenient laboratory in which to study MHD turbulence. Structure functions of the magnetic and velocity fields sampled from the solar wind have been constructed. These show that the scaling exponents ζ_p vary nonlinearly with p (Refs. 26–28) which is a signature of intermittency. Treatment of the raw PDFs also shows the intermittent quality of the solar wind in that their functional form changes with the length scale l.[27] This lack of global self-similarity is indicative of intermittency and has been studied[29] using the cascade model of Castaing *et al.*[30]

A currently favored model for intermittent turbulence is that of She and Leveque[13] (SL), which relates the scaling exponents ζ_p to the geometry of those structures that are most intensely dissipating. This argument relies on the refined similarity hypothesis, which provides a relationship between the assumed statistical self-similarity in the local rate of disspation and that found in $S^p(l)$. Applied to K41 and IK, this hypothesis can be recast in terms of ESS [recall Eq. (7)] as

$$S^p(l) \sim \langle \epsilon^{p/3}(l,\mathbf{x},t)\rangle (S^3(l))^{p/3}, \tag{10a}$$

$$S^p(l) \sim \langle \epsilon^{p/4}(l,\mathbf{x},t)\rangle (S^4(l))^{p/4}, \tag{10b}$$

after Eq. (12) in Ref. 22 and Eq. (10) in Ref. 24. Here, Eq. (10a) follows K41 while Eq. (10b) follows the IK phenomenology. Both relations imply ESS in the local rate of dissipation, given the existence of ESS in the fluid and field variables as in Eq. (7); this was recently recovered for the 3D incompressible MHD decaying turbulence simulation of Biskamp and Müller and was found[17] to agree with their SL model. However, it was not possible to verify Eq. (10), which links the scaling of dissipative and Elsässer variables, to high order (high p). The present work investigates this relationship.

TABLE I. Parameters of driven turbulence runs. N^2 is the number of the grid points, P/T_{NL} is the time period over which the steady state is tracked in terms of the nonlinear turnover time, L_0/l_d is the ratio of the simulation box length to the Kolmogorov dissipation scale, and R_v is the kinetic Reynolds number. Statistics are calculated from snapshots taken approximately every two nonlinear turnover times. The steady-state kinetic energy is approximately twice that of the magnetic energy. The viscosity μ is set equal to the magnetic diffusivity η making the magnetic and kinetic Reynolds numbers equal and the magnetic Prandtl number equal to unity. The rms sonic Mach number is $\simeq 0.2$ and the steady-state rms fluctuations in density are $\simeq 0.1$ for all runs.

Run No.	N	P/T_{NL}	L_0/l_d	R_v
1	512	99	530	372
2	1024	107	930	790
3	2048	114	1800	2000
4	4096	114	2900	4100

III. NUMERICAL PROCEDURE

The 2D isothermal MHD equations with a constant sound speed c_s are solved on a periodic square grid using a finite difference method[31] which is sixth order in space and fourth order in time. The equations are, in physical units,

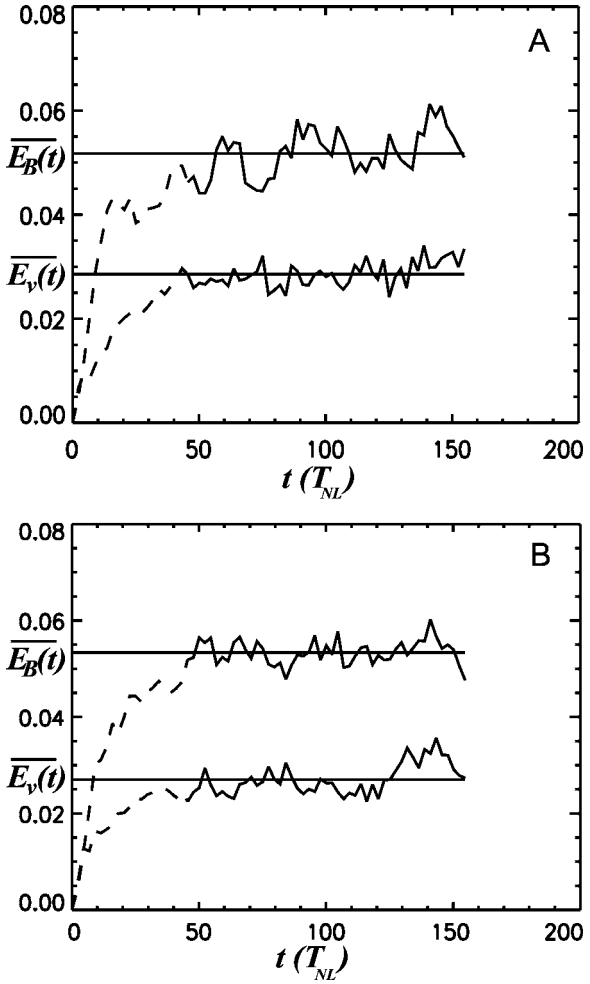

FIG. 1. The temporal evolution of the space averaged kinetic energy $\overline{E_v}=\overline{\rho v^2}/2$ (lower curve) and magnetic energy $\overline{E_B}=\overline{B^2}/2$ (upper curve) for runs 4 (panel a) and 3 (panel b) (see Table I). The solid part of the curves shows the period over which steady-state averages are calculated. The horizontal lines show the time averages calculated over this period. The broken part of the curves shows the temporal evolution before steady-state averages are calculated.

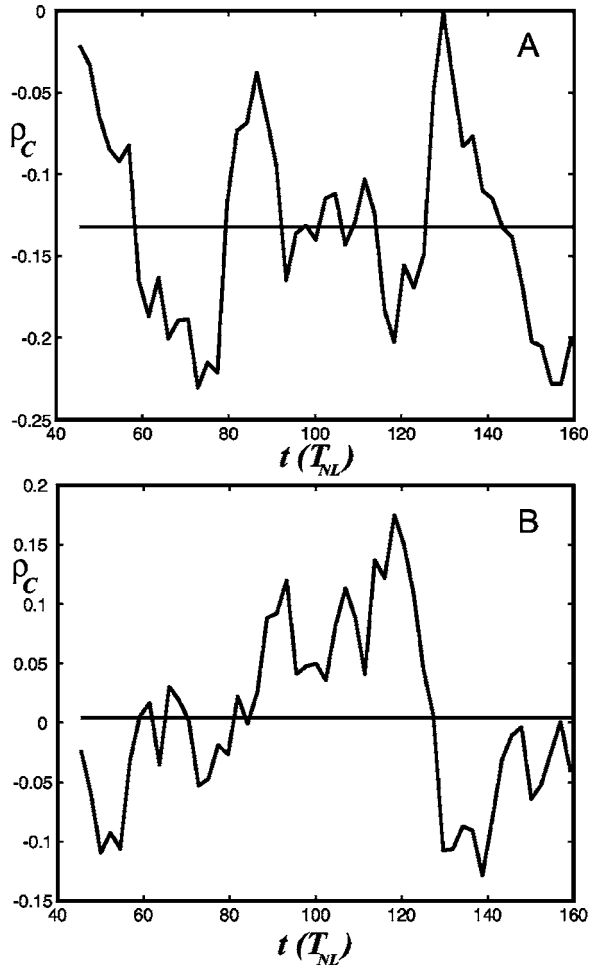

FIG. 2. The temporal evolution of the alignment of the velocity and magnetic fields $\rho_C(t)$ for runs 4 (panel a) and 3 (panel b) (see Table I). The horizontal lines show the time averages calculated over this period.

$$\rho\left(\frac{\partial \mathbf{v}}{\partial t}+(\mathbf{v}\cdot\boldsymbol{\nabla})\mathbf{v}\right)=-c_s^2\,\boldsymbol{\nabla}\rho+\mathbf{j}\wedge\mathbf{B}+\mu\left(\nabla^2\mathbf{v}+\frac{1}{3}\boldsymbol{\nabla}(\boldsymbol{\nabla}\cdot\mathbf{v})\right)+\mathbf{f}_v, \tag{11}$$

$$\frac{\partial \rho}{\partial t}+\nabla(\rho\mathbf{v})=0, \tag{12}$$

$$\frac{\partial \mathbf{B}}{\partial t}=\boldsymbol{\nabla}\wedge(\mathbf{v}\wedge\mathbf{B})+\eta\nabla^2\mathbf{B}+\mathbf{f}_B. \tag{13}$$

Here ρ is the fluid density; $\mathbf{B}$ is the magnetic field; $\mathbf{j}$ is the current density; $\mu=\nu\rho$, where ν is the kinematic viscosity; η is the magnetic diffusivity; $\mathbf{f}_v$ and $\mathbf{f}_B$ are the forcing functions for the velocity field and magnetic field, respectively. These equations are physically relevant to plasma turbulence, where the perturbed magnetic field is small compared to the mean magnetic field and is essentially perpendicular to it. The code's nonlinear behavior is tested for robustness against that of a previously published scheme[32] by performing decaying turbulence test runs (see Appendix).

Our principal results are derived from driven isothermal simulations. We drive the simulations so as to maximize our ability to obtain statistics over many eddy turnover times. Compared to decaying simulations, however, driven simulations usually require longer run times to obtain reliable statistics since temporal fluctuations are greater.[7] An isothermal scheme is convenient when considering driven simulations, in order to avoid the problem of continual heating, and the resulting continual increase in sound speed, which arises in codes that solve an equation of state. Thus a radiation function does not need to be considered.

We shall discuss the results of four simulations (see Table I) with N ranging from 512 to 4096. We drive the simulations isotropically in the wave-number shell $k_0\pm0.5$ and set $k_0=4$ to allow the development of the inverse cascade. Both the induction equation and the equation of motion are driven in line with previous studies,[8,9] noting that there is no dynamo action in 2D (see, e.g., Ref. 20). The driving functions $\mathbf{f}_v$ and $\mathbf{f}_B$ are updated every time step. They force shear (i.e., solenoidal) modes of random phase and orientation whose amplitude is proportional to $k_0\sqrt{k/\delta t}$, where δt is the variable time discretization of the solver. The constant of

TABLE II. Ratios of scaling exponents calculated from the Elsässer field variables for different runs (see Table I). Errors are an estimate of the possible range of straight line fits that can be drawn on the ESS plots (see Fig. 4).

Run No.	1	2	3	4
ζ_1^+/ζ_3^+	$0.39^{\leqslant 0.39}_{\geqslant 0.38}$	$0.40^{\leqslant 0.41}_{\geqslant 0.40}$	$0.42^{\leqslant 0.42}_{\geqslant 0.41}$	$0.42^{\leqslant 0.43}_{\geqslant 0.42}$
ζ_2^+/ζ_3^+	$0.73^{\leqslant 0.74}_{\geqslant 0.71}$	$0.74^{\leqslant 0.75}_{\geqslant 0.73}$	$0.75^{\leqslant 0.76}_{\geqslant 0.74}$	$0.76^{\leqslant 0.77}_{\geqslant 0.75}$
ζ_4^+/ζ_3^+	$1.21^{\leqslant 1.24}_{\geqslant 1.19}$	$1.18^{\leqslant 1.21}_{\geqslant 1.15}$	$1.16^{\leqslant 1.19}_{\geqslant 1.14}$	$1.16^{\leqslant 1.17}_{\geqslant 1.14}$
ζ_5^+/ζ_3^+	$1.37^{\leqslant 1.42}_{\geqslant 1.33}$	$1.31^{\leqslant 1.35}_{\geqslant 1.27}$	$1.26^{\leqslant 1.30}_{\geqslant 1.22}$	$1.25^{\leqslant 1.27}_{\geqslant 1.22}$
ζ_6^+/ζ_3^+	$1.50^{\leqslant 1.57}_{\geqslant 1.43}$	$1.40^{\leqslant 1.45}_{\geqslant 1.34}$	$1.30^{\leqslant 1.36}_{\geqslant 1.25}$	$1.30^{\leqslant 1.34}_{\geqslant 1.26}$
ζ_1^-/ζ_3^-	$0.39^{\leqslant 0.39}_{\geqslant 0.38}$	$0.40^{\leqslant 0.41}_{\geqslant 0.40}$	$0.41^{\leqslant 0.42}_{\geqslant 0.41}$	$0.42^{\leqslant 0.43}_{\geqslant 0.42}$
ζ_2^-/ζ_3^-	$0.73^{\leqslant 0.74}_{\geqslant 0.71}$	$0.74^{\leqslant 0.75}_{\geqslant 0.73}$	$0.75^{\leqslant 0.76}_{\geqslant 0.74}$	$0.76^{\leqslant 0.77}_{\geqslant 0.75}$
ζ_4^-/ζ_3^-	$1.21^{\leqslant 1.24}_{\geqslant 1.18}$	$1.19^{\leqslant 1.22}_{\geqslant 1.16}$	$1.17^{\leqslant 1.20}_{\geqslant 1.14}$	$1.16^{\leqslant 1.17}_{\geqslant 1.14}$
ζ_5^-/ζ_3^-	$1.36^{\leqslant 1.40}_{\geqslant 1.32}$	$1.32^{\leqslant 1.36}_{\geqslant 1.28}$	$1.27^{\leqslant 1.31}_{\geqslant 1.23}$	$1.25^{\leqslant 1.28}_{\geqslant 1.22}$
ζ_6^-/ζ_3^-	$1.48^{\leqslant 1.54}_{\geqslant 1.43}$	$1.42^{\leqslant 1.48}_{\geqslant 1.37}$	$1.33^{\leqslant 1.38}_{\geqslant 1.28}$	$1.30^{\leqslant 1.34}_{\geqslant 1.26}$

proportionality is the same for both $\mathbf{f}_B$ and $\mathbf{f}_v$. Importantly, the amplitude is chosen to be proportional to $\sqrt{1/\delta t}$ so that the time-integrated power of the forcing functions is independent of δt (Ref. 14)—δt being a quantity that can vary throughout the simulation. The phases and orientations of $\mathbf{f}_v$ and $\mathbf{f}_B$ are chosen independently. A method of driving often used in hydrodynamic turbulence is to fix the amplitude of the lowest Fourier modes to a predetermined value whilst letting their relative phases evolve according to the equation of motion. However, we find that if we use this driving for $\mathbf{v}$ and $\mathbf{B}$, the MHD turbulent dynamics are suppressed by a combination of the inverse cascade and the process of dynamic alignment. This culminates in the formation of a magnetic vortex and an aligned or antialigned velocity vortex on the scale of the simulation domain. Studies concerning the evolution of the Orszag-Tang vortex have shown that the dynamic alignment process is present in both incompressible and compressible MHD turbulences.[33,34] These studies find that this process is hindered as the Mach number increases. However, for Mach numbers of $\simeq 0.2$, as in the present case, there is little difference between the compressible and incompressible cases.[33] We find that driving around the wave vector $k_0=4\pm 0.5$ allows the inverse cascade to evolve without the condensation of structures on the largest scale. The randomization of the driving phase inhibits the dynamic alignment of the velocity and magnetic fields. The simulation is driven in this manner from initial conditions of $\rho=1$, $\mathbf{v}=\mathbf{B}=0$, and $c_s=1$. The simulation evolves into a state such that the magnetic and kinetic energies fluctuate about a well-defined mean with time. This is termed steady state. The steady-state magnetic energy is found to be approximately twice the steady-state kinetic energy. An excess of magnetic energy is also found in the driven 2D simulations of Refs.8,9. The temporal evolution of the space averaged kinetic energy $\overline{E_v}=\overline{\rho v^2}/2$ and magnetic energy $\overline{E_B}=\overline{B^2}/2$ for runs 3 and 4 (see Table I) are shown in Fig. 1. The quasi-steady-state shown here should be compared with that found in other similar investigations, e.g., Fig. 1 of Ref. 9.

Statistics are then calculated from snapshots separated by approximately two nonlinear turnover times $T_{\mathrm{NL}}=1/(k_0\langle E\rangle^{1/2})$ within this steady state, where $\langle E\rangle=\langle\frac{1}{2}(B^2+\bar{\rho}v^2)\rangle$. The field alignment of the magnetic and velocity fields, defined here as $\rho_C(t)=\overline{2(\mathbf{v}\cdot\mathbf{B})}/\overline{(v^2+B^2)}$, is also an important parameter in characterizing MHD turbulence. The temporal evolution of ρ_C is given in Fig. 2. Oscillations with a period of many nonlinear turnover times exist in ρ_C for both runs shown. This illustrates the need to perform time averaging over many tens of nonlinear turnover times to achieve reliable statistics. The time average of ρ_C varies for each run but is below 0.15 in every case (compare the value of $\simeq 0.16$ reported in Ref. 9) and can be as low as 0.004 as shown in Fig. 2. It is found that different values of this time average can be achieved by driving the simulations with different sets of random numbers, though the recovered scaling exponents (as in Tables II and III) remain constant to within errors. We thus conclude that the levels of field cor-

TABLE III. Test of the refined similarity hypothesis as modified for consistency with extended self-similarity. K41 or IK refers to Eqs. (10a) and (10b), respectively. The symbols + or − represent scaling derived from the $\mathbf{z}^+$ and $\mathbf{z}^-$ Elsässer field variables, respectively. Exact agreement would be indicated by a value of 1.0 across all columns.

	Run 3					
	$p=1$	$p=2$	$p=3$	$p=4$	$p=5$	$p=6$
K41+	$1.05^{\leqslant 1.07}_{\geqslant 1.04}$	$1.04^{\leqslant 1.05}_{\geqslant 1.02}$	⋯	$0.95^{\leqslant 0.97}_{\geqslant 0.93}$	$0.90^{\leqslant 0.93}_{\geqslant 0.88}$	$0.86^{\leqslant 0.90}_{\geqslant 0.83}$
K41−	$1.05^{\leqslant 1.07}_{\geqslant 1.04}$	$1.04^{\leqslant 1.05}_{\geqslant 1.02}$	⋯	$0.96^{\leqslant 0.98}_{\geqslant 0.94}$	$0.92^{\leqslant 0.94}_{\geqslant 0.89}$	$0.88^{\leqslant 0.91}_{\geqslant 0.85}$
IK+	$1.20^{\leqslant 1.21}_{\geqslant 1.18}$	$1.15^{\leqslant 1.17}_{\geqslant 1.13}$	$1.08^{\leqslant 1.10}_{\geqslant 1.06}$	⋯	$0.92^{\leqslant 0.95}_{\geqslant 0.90}$	$0.86^{\leqslant 0.89}_{\geqslant 0.83}$
IK−	$1.19^{\leqslant 1.20}_{\geqslant 1.17}$	$1.14^{\leqslant 1.16}_{\geqslant 1.12}$	$1.07^{\leqslant 1.09}_{\geqslant 1.05}$	⋯	$0.93^{\leqslant 0.96}_{\geqslant 0.91}$	$0.88^{\leqslant 0.91}_{\geqslant 0.85}$
	Run 4					
	$p=1$	$p=2$	$p=3$	$p=4$	$p=5$	$p=6$
K41+	$1.06^{\leqslant 1.07}_{\geqslant 1.06}$	$1.04^{\leqslant 1.05}_{\geqslant 1.04}$	⋯	$0.95^{\leqslant 0.96}_{\geqslant 0.94}$	$0.90^{\leqslant 0.92}_{\geqslant 0.88}$	$0.85^{\leqslant 0.91}_{\geqslant 0.82}$
K41−	$1.07^{\leqslant 1.07}_{\geqslant 1.06}$	$1.04^{\leqslant 1.05}_{\geqslant 1.04}$	⋯	$0.95^{\leqslant 0.96}_{\geqslant 0.94}$	$0.90^{\leqslant 0.92}_{\geqslant 0.89}$	$0.86^{\leqslant 0.88}_{\geqslant 0.85}$
IK+	$1.20^{\leqslant 1.21}_{\geqslant 1.20}$	$1.15^{\leqslant 1.16}_{\geqslant 1.15}$	$1.07^{\leqslant 1.09}_{\geqslant 1.07}$	⋯	$0.93^{\leqslant 0.95}_{\geqslant 0.90}$	$0.87^{\leqslant 0.91}_{\geqslant 0.84}$
IK−	$1.21^{\leqslant 1.21}_{\geqslant 1.20}$	$1.16^{\leqslant 1.16}_{\geqslant 1.15}$	$1.08^{\leqslant 1.09}_{\geqslant 1.07}$	⋯	$0.93^{\leqslant 0.94}_{\geqslant 0.91}$	$0.88^{\leqslant 0.89}_{\geqslant 0.86}$

relation present here do not lead to the significant weakening of nonlinear dynamics and any variation present between runs does not affect the cascade process significantly. Nondimensional parameters for the runs performed are summarized in Table I.

Steady-state averages are calculated from every point in the simulation grid with the differencing vector $\mathbf{l}$ lying in the x and then y directions. We then take a temporal average from snapshots separated by a constant time increment, which is approximately $2T_{\mathrm{NL}}$ for all runs. The number of snapshots taken in the period of steady state for all runs is approximately 50. This leads to the total number of data points being considered for each average to be approximately $2\times N^2\times 50$ which gives $\simeq 4.2\times 10^8$ points for run 3 and $\simeq 1.7\times 10^9$ points for run 4. The rms sonic Mach number for all runs is $\simeq 0.2$ though locally the Mach number can exceed this value, e.g., for our data sets, the highest local Mach number (defined as $|\mathbf{v}|/c_s$) is 1.47 for run 4 and 1.32 for run 3.

IV. RESULTS

First we establish the extent of statistical convergence as the Reynolds number is increased. This involves establishing the appropriate scaling range for ESS and then noting how the ratio of scaling exponents $\zeta_p^{\pm}/\zeta_3^{\pm}$ varies with the Reynolds number. It has been found from experiment that the ESS scaling range should extend down to approximately $5l_d$.[22,23] The K41 and IK phenomenologies made different predictions for the dissipation scale l_d,[4] which we denote as l_{K41} and l_{IK}, respectively. For a magnetic Prandtl number of unity, as in the present case, $l_{\mathrm{K41}}=(\nu^3/\langle\epsilon\rangle)^{1/4}$ and $l_{\mathrm{IK}}=(\nu^2 v_A/\langle\epsilon\rangle)^{1/3}$. Here $\langle\epsilon\rangle$ is the average viscous plus Ohmic rates of dissipation and v_A is the characteriztic Alfvén speed. Thus the ESS scaling range, shown in Fig. 3, gives some insight into the appropriate phenomenology. These plots suggest that scaling only extends down to $5l_{\mathrm{IK}}$ and breaks before $5l_{\mathrm{K41}}$. This suggests that the energy cascade time may be modified by the presence of Alfvén waves, which leads to the IK phenomenology. From here on, all references to measured $\zeta_p^{\pm}/\zeta_3^{\pm}$ are related to values calculated within the scaling range established in Fig. 3.

Examples of ESS scaling for run 4 are shown in Fig. 4. We perform ESS analysis on the structure functions $S_{\pm}^p$ and present values of $\zeta_p^{\pm}/\zeta_3^{\pm}$ in Table II, inferred using Eq. (7). Also shown in Table II is an estimate of the possible range of straight line fits that can be drawn on the ESS plots (see Fig. 4). This gives a guide to the level of statistical error present in the calculation of $\zeta_p^{\pm}/\zeta_3^{\pm}$. Values of $\zeta_p^{\pm}/\zeta_3^{\pm}$ recovered from the $\mathbf{z}^+$ and $\mathbf{z}^-$ fields agree well with each other, particularly for run 4. This reflects the low degree of field alignment present in these simulations. There is an apparent trend in the values of the scaling exponents as the Reynolds number increases. This trend is upward for $p<3$ and downward for $p>3$, however, it is very weak from run 3 to 4 in comparison with the level of statistical error present. Encouragingly this suggests the onset of statistical convergence for $R_v>2000$, and we therefore focus our subsequent analysis on the results of runs 3 and 4.

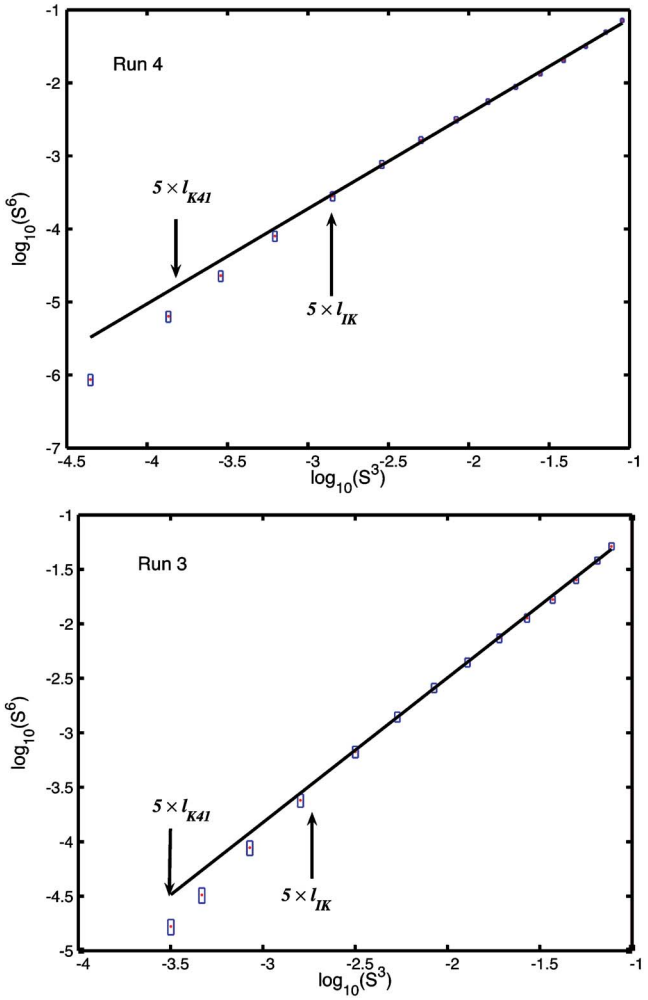

FIG. 3. ESS scaling in the $\mathbf{z}^-$ field, order 6 against order 3. The boxes surrounding the data points indicate the standard error present in the time averaging process. Marked on the plots are the approximate values of $S_-^3(l=5l_{\mathrm{IK}})$ and $S_-^3(l=5l_{\mathrm{K41}})$. Benzi *et al.* (Refs. 22,23) found that ESS scaling should extend down to approximately $5l_d$. The break in scaling occurs at approximately $S_-^3(l=5l_{\mathrm{IK}})$ in these plots, showing that the viscous cutoff of the cascade is higher than expected from Kolmogorov phenomenology (K41) and is closer to that of Iroshnikov and Kraichnan (IK).

We now discuss the relevance of the scaling exponents recovered here when compared to those reported in Refs. 7,8. First we emphasize that such a direct comparison is somewhat affected by the fact that both the studies in Refs. 7,8 concern incompressible turbulence, whereas our results come from weakly compressible runs with sonic Mach number $\simeq 0.2$. However, we anticipate that the effect of compressibility on the values of the scaling exponents is low for Mach numbers less than 1, as found in the transonic driven simulations of Ref. 35 and in the time evolution of global quantities in the Orszag-Tang vortex.[33,34] Our results are in general agreement with those reported in Refs. 7,8 in that, as shown in Fig. 5, the values of $\zeta_p^{\pm}/\zeta_3^{\pm}$ corresponding to 2D MHD turbulence are lower than those corresponding to 3D decaying MHD turbulence when $p>3$ and higher when $p<3$. The values of $\zeta_p^{\pm}/\zeta_3^{\pm}$ reported here agree with those found in the 2D decaying incompressible runs of Ref. 7 to within statistical error for $p\leqslant 4$, though they diverge from

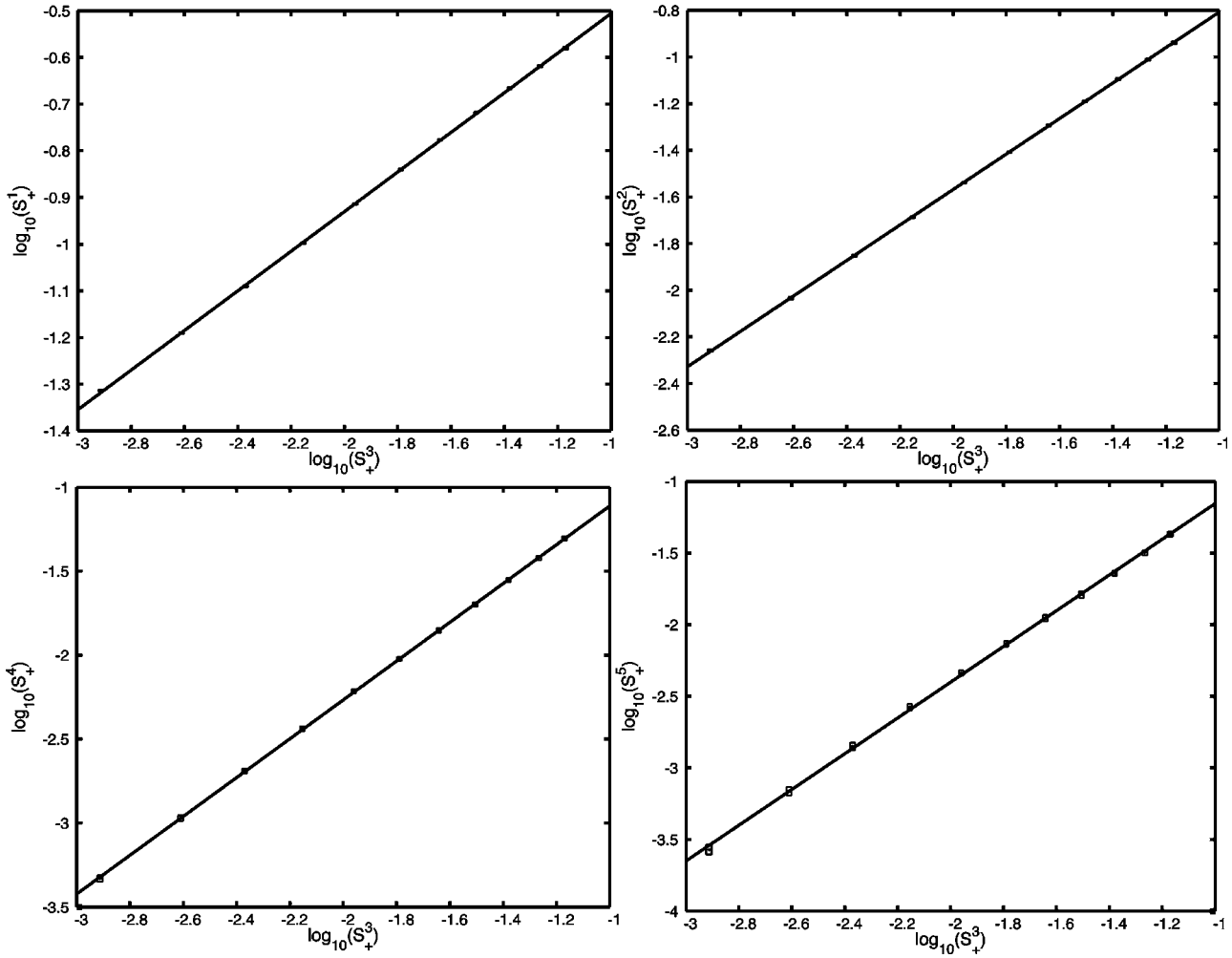

FIG. 4. ESS scaling of $\mathbf{z}^+$ Elsässer field variables [compare Eq. (7) with $q=3$ and $p=1-5$] for run 4. We exclude $p=3$ since this necessarily gives perfect scaling. The boxes surrounding the data points indicate the standard error present in the time averaging process. See column 4 of Table II for the corresponding inferrred values of ζ_p^+/ζ_3^+.

these values for $p>4$. We now consider the scaling exponents reported in Ref. 8 for 2D-driven incompressible turbulence. Figure 5 shows that the scaling exponents recovered in the driven 2D simulation of Ref. 8 follow the same trend as those calculated here in run 4 (the exponents recovered in run 3 being practically the same). Figure 5 further suggests that the values of ζ_p^+/ζ_3^+ from driven 2D MHD turbulence diverge with increasing p from those values obtained from decaying turbulence, the values of ζ_p^+/ζ_3^+ being smaller in the driven case than in the decaying.

Results concerning the scaling of the time averaged total energy spectra are shown in Fig. 6. We expect to recover a power law that should be present in both runs 3 and 4, and should extend to higher k in run 4, which is performed at a higher Reynolds number. We fit a power law to the inertial range interval of these plots and find that it has an index that lies somewhere between the $-5/3$ predicted by K41 and the $-3/2$ predicted by IK. This can be seen in Fig. 6 which displays $E(k)k^{5/3}$ [Fig. 6(a)] and $E(k)k^{3/2}$ [Fig. 6(b)] for runs 3 and 4, with the index found by the power-law fit indicated by bold lines. The scaling range in run 4 can be seen to extend to somewhat higher k than that of run 3. The fact that

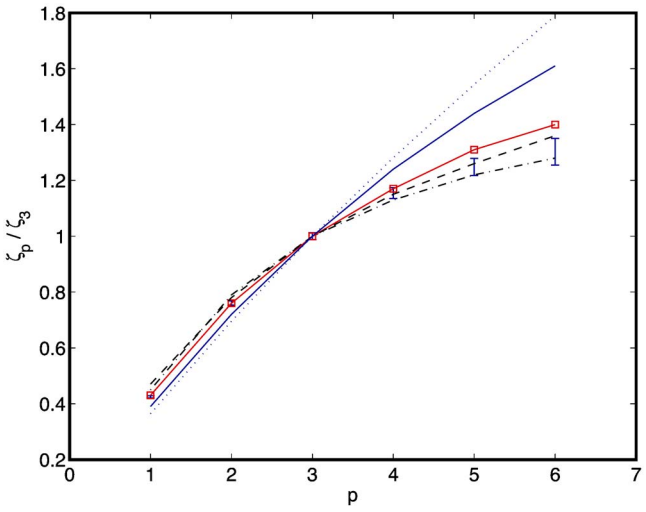

FIG. 5. Relative scaling exponents ζ_p/ζ_3 obtained from the driven 2D simulation of run 4 (error bars), the driven 2D simulation of Ref. 8 (upper broken line ζ_p^+/ζ_3^+, lower broken line ζ_p^-/ζ_3^-), and the 2D decaying simulation of Ref. 7 (solid line with square markers). Values reported from the 3D decaying simulation of Ref. 10 (solid line) and the MHD intermittency model of Politano and Pouquet (Ref. 12) (dotted line) are shown for comparison.

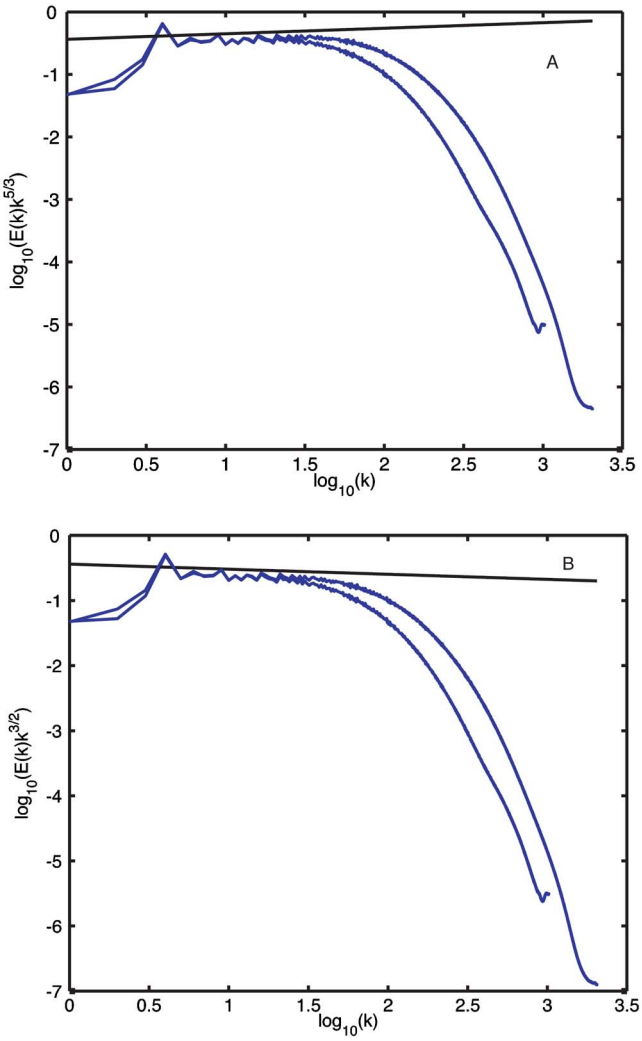

FIG. 6. Time-averaged energy spectra [compare Eq. (3)] for high-resolution runs 3 (lower) and 4 (upper). The vertical axis is normalized by $k^{5/3}$ (a) and $k^{3/2}$ (b). The bold lines indicate the power-law index as estimated by a power-law fit over the inertial range. It can be seen that the power law has a negative index whose magnitude is less than the 5/3 predicted by K41 but is greater than the 3/2 predicted by IK. The scaling range is extended to higher k for run 4 compared to run 3, since run 4 is performed at a higher Reynolds number.

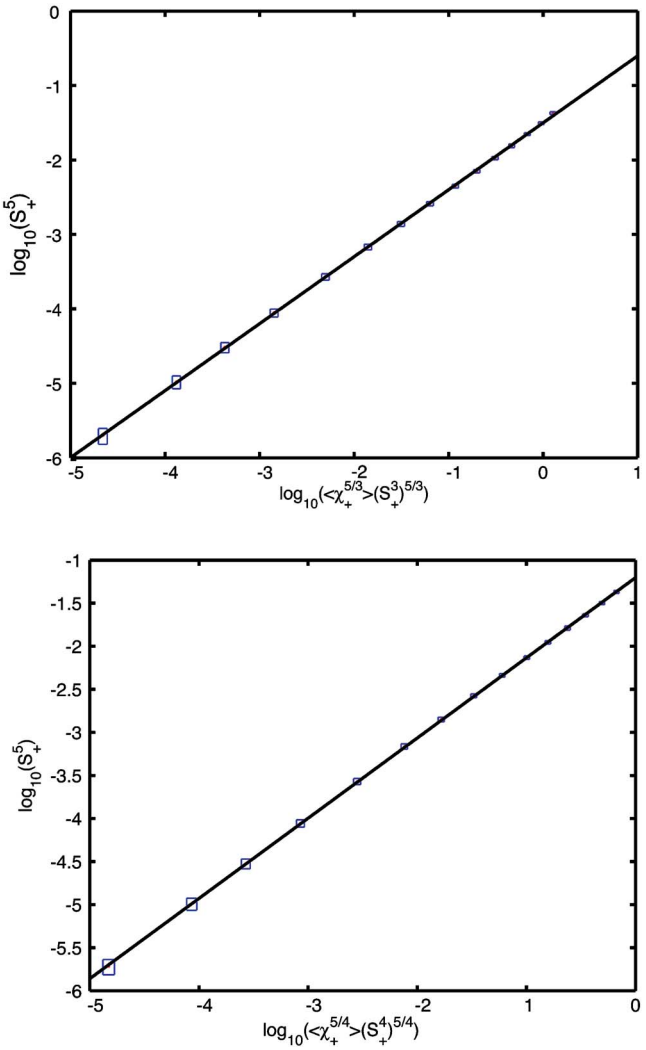

FIG. 7. Scaling of the ESS-consistent refined similarity hypothesis for the Kolmogorov case [compare Eq. (10a)] (top) and the IK case [compare Eq. (10b)] (bottom) for run 4, order $p=5$. Here the scaling range extends to below $5l_d$ as found in Ref. 23. However, the ideal gradient of unity is not recovered, see Table III. The boxes surrounding the data points indicate the standard error present in the time averaging process.

the power law has a negative index whose magnitude is less than 5/3 supports the hypothesis that the energy cascade is modified by the presence of Alfvén waves, as found in our investigation of the ESS scaling range.

We now present results concerning the ESS-modified refined similarity hypothesis Eq. (10). Here we approximate $\langle \epsilon(l)^p \rangle$ by calculating $\langle \chi_{\pm}(l)^p \rangle$ directly from the simulations. It has been found that this scaling should persist to length scales as small as l_d.[23] Since we have not calculated statistics for $l < l_{\mathrm{K41}}$ (recall $l_{\mathrm{K41}} < l_{\mathrm{IK}}$), scaling should therefore apply across our entire data set. Indeed we find excellent scaling for both forms of the hypothesis down to the smallest scale we measure, see Fig. 7.

The family of plots of the type shown in Fig. 7, see Eq. (10), that can be constructed by varying p should all have a gradient of unity, given the correct scaling law. Hence only one of the K41 or the IK formulations of Eq. (10), that is Eq. (10a) or (10b), should return a value close to unity, whilst the other version should not. By this method we can aim to validate one scaling hypothesis over the other, given sufficiently small statistical error. The gradients we obtain for Eqs. (10a) and (10b) when plotted on a log-log scale are tabulated in Table III.

We find good statistical convergence between runs 3 and 4. Furthermore, we find that no statistical distinction can be drawn between results derived from the $\mathbf{z}^+$ and $\mathbf{z}^-$ Elsässer fields. Table III shows a trend in the recovered gradient as p is varied for both Eqs. (10a) and (10b), that is, for both K41 and IK phenomenologies. Neither scaling hypothesis is consistent with this behavior. However, we have greater statistical confidence in our low-order results. These suggest that the K41 case of the refined similarity hypothesis [Eq. (10a)] is more appropriate for 2D MHD turbulence than the IK case.

V. CONCLUSIONS

We have developed a high-order finite difference code to study driven 2D MHD turbulence and have performed runs at Reynolds numbers that are high enough to achieve statistical convergence. These yield ESS scaling in the Elsässer field variables. The extent of the ESS scaling suggests that dissipation occurs at a larger length scale than that expected from K41 phenomenology (nonlinear interaction via random eddy scrambling[1]) and is closer to that expected from IK (nonlinear interaction via Alfvén wave collisions[2,3]). This gives some support to the idea that the energy cascade is modified by the presence of Alfvén waves, as suggested by the IK phenomenology. The values of $\zeta_p^{\pm}/\zeta_3^{\pm}$ are in general agreement with previous studies, in that greater spatial intermittency of turbulent activity is implied than for the 3D decaying case.[7,8,10] This is consistent with the finding in Ref. 36 which recovers this phenomenon when a strong mean magnetic field is applied to a 3D simulation, suggesting that the presence of a strong field causes the 3D statistics to become more intermittent and thus quasi-2D. We obtain values of the scaling exponent ratios $\zeta_p^{\pm}/\zeta_3^{\pm}$ that follow those found in the driven simulation of Ref. 8 as p increases and are generally smaller than those shown in the decaying runs of Ref. 7 for $p>3$. Further investigation is needed to confirm the hypothesis that statistics gathered from 2D quasistationary driven MHD turbulence may differ in a consistent way from those taken from decaying turbulence. The time averaged total-energy spectra recovered from these runs show that the power law has a negative index whose magnitude is less than the classic Kolmogorov (K41) prediction, again suggesting that the cascade differs from the 3D hydrodynamic and MHD cases which are well modeled by K41.

We have extended our previous investigation,[17] which is related to 3D incompressible MHD turbulence, to consider whether the scaling of the Elsässer field variables for compressible 2D MHD turbulence is consistent with an SL interpretation based on a refined similarity hypothesis. Development of our new simulation has enabled us to address the combined scaling properties of dissipation and field variables, which is difficult computationally in the 3D case. We find that the ESS-adjusted refined similarity hypothesis Eq. (10) can be tested directly using our 2D simulation. To our knowledge this is the first time that scaling of this type, which Benzi *et al.* decribed as a generalization of Kolmogorov's refined similarity hypothesis,[23] has been recovered for MHD turbulence. Neither the K41 nor IK scaling hypotheses agree with our numerical results to within errors, which are sufficiently low to distinguish between them. However, the low-order investigations, for which statistical confidence levels are higher, are better approximated by the K41 scaling hypothesis than by that of IK.

An interesting theoretical situation now presents itself. There is considerable evidence from this study and others that the K41 phenomenology is not appropriate when considering 2D MHD turbulence.[7,8,11] However, the IK phenomenology is not adequate either, since no IK-based model that incorporates intermittency has been successfully applied to the scaling exponents $\zeta_p^{\pm}$. The apparent inadequacy of both of the scaling expressions in Eq. (10), which represent the ESS-adjusted refined similarity hypothesis, is intriguing since a self-consistent SL-based model cannot be constructed without a formulation of this type. This will be the subject of further work.

ACKNOWLEDGMENTS

This work was supported in part by the Engineering and Physical Sciences Research Council through a CASE scholarship with the United Kingdom Atomic Energy Authority. The computing facilities were provided by the Centre for Scientific Computing of the University of Warwick with support from a Science Research Investment Fund grant.

APPENDIX: CODE COMPARISON

The linear behavior of the scheme we use here, which is fourth order in time and sixth order in space, can be tested by setting the forcing functions in Eqs. (11) and (13) to zero and initializing with a linear mode (sonic, Alfvénic or magnetosonic). This was tested extensively in the development stage of the code. Confidence in the results obtained from this scheme relies on the robustness of its nonlinear behavior and the use of the isothermal approximation. As such, we test this high-order scheme against the Lagrangian remap scheme of Ref. 32 which implements an equation of state with no forcing functions. We set the forcing functions in Eqs. (11) and (13) to zero and initialize both schemes with an out-of-equilibrium distribution that has a power spectrum $E_v \sim E_B \sim k^2 \exp[-(k^2/k_0^2)]$ with $k_0=4$; the phases of the $\mathbf{v}$ and $\mathbf{B}$ modes are randomized and the initial conditions $\nabla\cdot\mathbf{v}=0$ and $\nabla\cdot\mathbf{B}=0$ are imposed. The term k_0 represents the dominant wave number in the initial distribution and is set to 4 to allow the development of the inverse cascade whilst still sufficiently resolving the small scale dynamics as in Refs. 7,10. The total magnetic plus kinetic energy in the simulation domain is initialized to unity. The density is initialized to a constant value of unity for both codes; we impose $c_s=1$ for the high-order code and the temperature is set to a constant value that ensures that $c_s=1$ for the Lagrangian code. Both schemes are solved on a 1024^2 grid. We evolve both schemes for five large eddy turnover times T, defined as the time it takes for the simulation to reach its maximum rate of energy dissipation following Ref. 10 [this period is approximately equivalent to twenty initial nonlinear turnover times (T_{NL} at $t=0$) for future reference]. Time invariance for decaying turbulence is simulated by the transformation $k' \rightarrow kl_d$ and $E' \rightarrow E/(\epsilon\nu^5)^{1/4}$. We find that power-law scaling of the energy spectrum is present for both runs after approximately $1.5T$, and persists for as long as we follow the evolution. Figure 8 shows the scatter plots of the normalized spectra for the time interval from $1.5T$ to $5T$.

Both spectra exhibit a power-law scaling consistent with Kolmogorov's prediction[1] and display many of the same features. The spectra differ at the highest wave numbers where spectra obtained from the high-order code display an upturn, while those obtained from the Lagrangian remap code do not. This is probably a consequence of the shock-capturing scheme implemented in the Lagrangian code, which damps

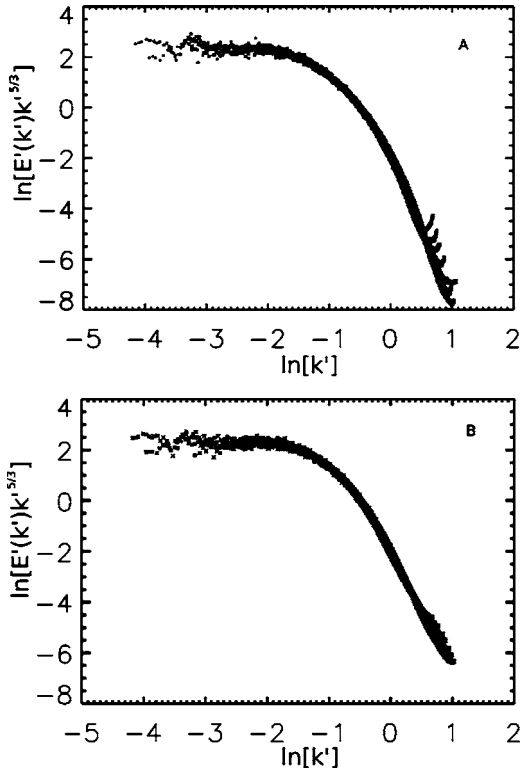

FIG. 8. Scatter plots of normalized energy spectra for decaying turbulence runs for the isothermal high-order code (a) and the Lagrangian remap code that solves an equation of state (b). The vertical axis is normalized by $k^{5/3}$.

high wave-number modes[32] and is not present in the high-order scheme. The overall level of agreement shows that the nonlinear interaction responsible for the development of the power law in the energy spectrum is robust against (i) changes in the detailed mechanics of the solver and (ii) the choice between using the isothermal approximation or implementing an equation of state. This demonstration is the main purpose of these decaying runs. We do not place great weight on the K41-type behavior of the normalized energy spectrum in Fig. 8 since it is possible to achieve power indices which approximate K41 and IK values by initializing the phases of the E_v and E_B Fourier modes with different sets of random numbers. That is, the K41 behavior shown here is for illustrative purposes only and does not represent a statistically reproducible result. We find that some memory of the initial conditions seems to persist for long periods for these decaying numerical experiments. We also note that the level of scatter present in the energy spectra of these decaying runs complicates the process of distinguishing between IK and K41 type spectra. In the present work we favor the high-order scheme since formally it is more accurate, although it has none of the shock-capturing capability of the Lagrangian remap code. As such, only runs with rms Mach numbers less than unity can be undertaken with the high-order scheme used here.

[1] A. N. Kolmogorov, Proc. R. Soc. London, Ser. A **434**, 9 (1991).
[2] P. S. Iroshnikov, Soviet Astronomy 7, 566 (1964).
[3] R. H. Kraichnan, Phys. Fluids **8**, 1385 (1965).
[4] W.-C. Müller and D. Biskamp, in *Turbulence and Magnetic Fields in Astrophysics*, edited by E. Falgarone and T. Passot (Springer, New York 2003), Vol. 614, pp. 3–26.
[5] P. Goldreich and S. Sridhar, Astrophys. J. **438**, 763 (1995).
[6] C. S. Ng, A. Bhattacharjee, K. Germaschewski, and S. Galtier, Phys. Plasmas **10**, 1954 (2003).
[7] D. Biskamp and E. Schwartz, Phys. Plasmas **8**, 3282 (2001).
[8] H. Politano, A. Pouquet, and V. Carbone, Europhys. Lett. **43**, 516 (1998).
[9] T. Gomez, H. Politano, and A. Pouquet, Phys. Fluids **11**, 2298 (1999).
[10] D. Biskamp and W.-C. Müller, Phys. Plasmas **7**, 4889 (2000).
[11] D. Biskamp and H. Welter, Phys. Fluids B **1**, 1964 (1989).
[12] H. Politano and A. Pouquet, Phys. Rev. E **52**, 636 (1995).
[13] Z.-S. She and E. Leveque, Phys. Rev. Lett. **72**, 336 (1994).
[14] N. E. L. Haugen, A. Brandenburg, and W. Dobler, Phys. Rev. E **70**, 016308 (2004).
[15] W.-C. Müller and D. Biskamp, Phys. Rev. Lett. **84**, 475 (2000).
[16] A. Bershadskii, Phys. Plasmas **10**, 4613 (2003).
[17] J. A. Merrifield, W.-C. Müller, S. C. Chapman, and R. O. Dendy, Phys. Plasmas **12**, 022301 (2005).
[18] D. Biskamp, *Magnetohydrodynamic Turbulence* (Cambridge University Press, Cambridge, UK, 2003).
[19] U. Frisch, *Turbulence* (Cambridge University Press, Cambridge, UK, 1995).
[20] D. Biskamp, *Nonlinear Magnetohydrodynamics* (Cambridge University Press, Cambridge, UK, 1993).
[21] R. Benzi, S. Ciliberto, R. Tripiccione, C. Baudet, F. Massaioli, and S. Succi, Phys. Rev. E **48**, R29 (1993).
[22] R. Benzi, S. Ciliberto, C. Baudet, and G. R. Chavarria, Physica D **80**, 385 (1995).
[23] R. Benzi, S. Ciliberto, C. Baudet, and G. Chavarria, Physica D **96**, 162 (1996).
[24] R. Benzi, M. V. Struglia, and R. Tripiccione, Phys. Rev. E **53**, R5565 (1996).
[25] M. L. Goldstein and D. A. Roberts, Phys. Plasmas **6**, 4154 (1999).
[26] L. F. Burlaga, J. Geophys. Res. **96**, 5847 (1991).
[27] E. Marsch and C.-Y. Tu, Nonlinear Processes Geophys. **4**, 101 (1997).
[28] T. S. Horbury and A. Balogh, Nonlinear Processes Geophys. **4**, 185 (1997).
[29] L. Sorriso-valvo, V. Carbone, P. Giuliani, P. Veltri, R. Bruno, V. Antoni, and E. Martines, Planet. Space Sci. **49**, 1193 (2001).
[30] B. Castaing, Y. Gangne, and E. J. Hopfinger, Physica D **46**, 177 (1990).
[31] J. D. Hoffman, *Numerical Methods for Engineers and Scientists* (McGraw-Hill, New York 1993).
[32] T. D. Arber, A. W. Longbottom, C. L. Gerrard, and A. M. Milne, J. Comput. Phys. **170**, 0151 (2001).
[33] R. B. Dahlburg and J. M. Picone, Phys. Fluids B **1**, 2153 (1989).
[34] J. M. Picone and R. B. Dahlburg, Phys. Fluids B **3**, 29 (1991).
[35] P. Padoan, R. Jimenez, A. Nordlund, and S. Boldyrev, Phys. Rev. Lett. **92**, 191102 (2004).
[36] W.-C. Müller, D. Biskamp, and R. Grappin, Phys. Rev. E **67**, 066302 (2003).